



Characterization of digital cameras based on photon transfer measurements

Carolina Alvarez, DESY, Germany

September 7, 2022

Abstract

Beam diagnostics devices are a fundamental part for any kind of accelerator. Imaging systems, such as area scan sensors, with high accuracy requirements are needed to operate beam monitors. In order to study the performance of such devices, photon transfer is a relevant testing methodology that makes it possible to obtain important camera parameters from a set of measurements. These parameters can characterize the camera performance based on standard criteria derived by the European Machine Vision Association. In this report, this procedure is performed on a CMOS camera, which will be characterized according to studies based on signal-to-noise and photon transfer measurements.

CONTENTS

I	Introduction	3
II	Video cameras in beam instrumentation	3
III	Theory of Characterization	4
i	Photon Transfer	4
ii	Signal to Noise Ratio	6
IV	Experimental Procedure	8
i	Equipment	8
ii	Setup	10
iii	Measurements	11
V	Analysis	11
i	Camera 1	11
ii	Camera 2	14
VI	Conclusions	15
	References	17

I. INTRODUCTION

Particle accelerators play an important role in a wide number of fields. More than 30,000 accelerators are in use around the world [1], while some are used for research, most of these devices are dedicated to industrial and medical applications.

Beam diagnostics, which are critical components of all particle accelerators, are responsible for quantifying the parameters of particle beams. They are an essential part to any kind of accelerator, and typically account for around 3-10% of the overall cost of a particle accelerator facility. They are required to provide highly accurate measurements of multiple parameters, and operate with fast response times.

A fundamental part of beam diagnostics are imaging systems, used for the purpose of measuring position, momentum, energy, or mass of charged particles [2]. They also provide useful information about the beam profile for machine optimization. These devices include area scan sensors, that provide the full two-dimensional information about the beam distribution, and make it possible to investigate shot-to-shot profile fluctuations. The study of these cameras will be the focus of this project.

II. VIDEO CAMERAS IN BEAM INSTRUMENTATION

In order to get high resolution beam profile measurements when using digital cameras, the conversion process from any charged particle in digital numbers by the data acquisition system must be linear, so that misinterpretation of measured beam sizes or shapes is avoided. It is also essential to make sure any resolution broadening induced by the physical mechanism or the optical system used in the measurements is small. This effects can be caused by different mechanisms, such as the noise introduced in the conversion from a photon distribution into a set of digital numbers in the camera.

This project will focus on the latter, and will aim to characterize the quality of an area scan camera used for beam profile diagnostics. The camera sensors to characterize can either be CCD or CMOS, both are commonly used in standard beam instrumentation applications [2], as can be seen in figure 1.

Both technologies provide semiconductor based arrays of pixels, however, there are some differences. CCD pixel act as capacitors, and their output is a charge which is converted to a digital signal by an external circuit, while CMOS uses in-pixel photo-diodes and integrated circuits, resulting in a voltage output. CCD imaging sensors have technically developed over the last 50 years to the point where the high-resolution formats with very low defect rates are available. CMOS sensors have become dominant over CCD sensors in consumer products like video, smart phone, and digital camera applications due to their low cost and fast readout speed. In the last years, also scientific CMOS (S-CMOS) sensors have been developed, and used for scientific research purposes. In this project, an industrial CMOS camera is to be considered.

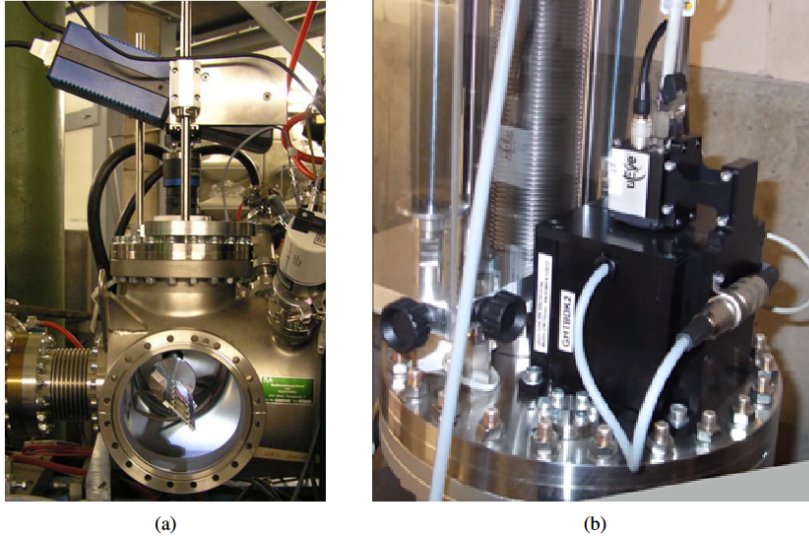


Figure 1: Scintillating screen for beam profile measurements at the GSI linear accelerator using a CCD camera (a) and one equipped with a CMOS camera in the high energy beam transfer line (b)

In order to characterize these cameras, the photon transfer (PT) is a valuable, widely applied testing methodology, whose basis will be described in the next section.

III. THEORY OF CHARACTERIZATION

i. Photon Transfer

Photon Transfer is a straightforward method to determine various sensor parameters by analyzing only two measured quantities: the average signal and noise. Following this method, the European Machine Vision Association derived the EMVA Standard 1288 [3], which is a unified method to measure, compute and present specification parameters and characterization data for cameras and image sensors used for machine vision application. It provides a concise definition and clear description of the measurement process, and will be followed in this report in order to characterize a digital camera.

This Standard can be applied as long as the camera under test fulfills several general assumptions, briefly listed here: (i) the amount of photons collected by a pixel depends on the radiative energy density, (ii) noise sources are stationary and white, (iii) only the total quantum efficiency is wavelength dependent, (iv) only the dark current depends on temperature, and (v) the sensor is linear.

The physical model used to portray a digital camera can be seen in figure 2 (a). It depicts a number of photons hitting a sensor pixel area during a certain exposure time, which, via the photoelectric effect, is trapped in a potential well, and creates a number

of electrons that form a charge. Such charge is converted to a voltage by a capacitor, which is later amplified and digitized, resulting in a digital grey value.

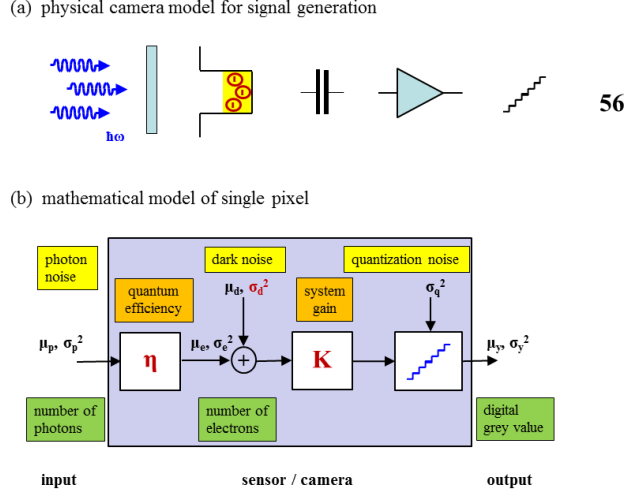


Figure 2: (a) Physical camera model for signal generation. (b) Mathematical model for a single pixel

The process taking place in a single pixel can also be described mathematically: during the exposure time, a number of incoming photons N_p hit its area. This number fluctuates statistically, and, according to the laws of quantum mechanics, the probability is Poisson distributed. Therefore the variance of the fluctuations is equal to the mean number of photons $\mu_p = \sigma_p^2$. A fraction of these photons given by the quantum efficiency η will be absorbed, generating photo electrons with a mean number of accumulated charges μ_e , and variance $\sigma_e^2 = \mu_e$. This variance can be rewritten in terms of the quantum efficiency and mean number of photons, $\sigma_e = \sqrt{\eta}\sigma_p$. As seen earlier, the accumulated charges are then converted into voltage, amplified, and transformed into a digital number. If all these processes are linear, they can be depicted by a black box where all the mechanisms are summarized in the so called overall system gain K , with units Digital Number (DN) per electrons. This mathematical model is represented in figure 2 (b).

Furthermore, thermal fluctuations can generate electron-hole pairs in the pixel. Similar to photon generated electron-hole pairs, the randomly generated electrons can be captured in the potential well, leading to noise (dark electrons). This effect is called dark current noise. With μ_d the mean dark electrons, the mean digital signal or grey value μ_y of the digital signal y can then be written as:

$$\mu_y = K(\mu_e + \mu_d) = k\eta\mu_p + \mu_{y,dark} \quad (1)$$

Where $\mu_{y,dark}$ indicates the mean dark signal coming from dark electrons.

Likewise, other noise sources can also contribute to the grey value. The temporal noise at one pixel, which is statistically independent from the noise at all other pixels, can also be characterized by its variance σ_i^2 , where i indicates an arbitrary noise source.

As mentioned previously, the number of charge units (electrons) fluctuates statistically, following a Poisson distribution, thus its variance is equal to the mean number of electrons $\sigma_e^2 = \mu_e$. This noise, often referred to as shot noise is given by the basic laws of physics and equal for all types of cameras.

All other noise sources depend on the specific sensor and camera electronic layout, and their variances add up in a linear way due to the linear signal model assumed by the EMVA 1288 Standard. When taking the camera as a black box as pictured in figure 2 (b), the additional noise sources to be considered are only two [3]:

- Noise sources related to sensor read out and amplifier circuits, which can be described by a signal-independent normal-distributed noise source with variance σ_d^2
- The noise source added by the final analog to digital conversion, which is uniform-distributed between the quantization intervals and has as variance of $\sigma_q^2 = \frac{1}{12}DN^2$.

The total variance σ_y^2 is then given by the laws of error propagation:

$$\sigma_y^2 = K^2(\sigma_d^2 + \sigma_e^2) + \sigma_q^2 \quad (2)$$

Then, using the dark noise variance to define $\sigma_{y,dark} = K\sigma_d$, equation 2 can be rewritten as:

$$\sigma_y^2 = K(\mu_y - \mu_{y,dark}) + \sigma_{y,dark}^2 \quad (3)$$

Where it is assumed that the contribution of the quantization noise in the analog-to-digital conversion ($\sigma_q^2 = \frac{1}{12}DN^2$) is negligible compared to the dark noise.

Equations 1 and 3 are the basis to the PT characterization, as they provide linear relations for the signal and noise, that, when compared and fitted with actual data, make it possible to experimentally access the camera's main parameters.

ii. Signal to Noise Ratio

To compute the quality of a detector signal, the Signal-to-Noise Ratio (SNR) is used. SNR is a measurement parameter in use in the fields of science and engineering that compares the level of the desired signal to the level of background noise, defined by:

$$SNR = \frac{\mu_y - \mu_{y,dark}}{\sigma_y} \quad (4)$$

It is usually expressed in bits, taking its base 2 logarithm $\log_2(SNR) = SNR_{bit}$. Using equations 1 and 3, it can be written as:

$$SNR_{bit} = \log_2(\eta) + \log_2(\mu_p) - \frac{1}{2}\log_2(\eta\mu_p + \sigma_d^2) \quad (5)$$

In the case of an ideal sensor with quantum efficiency $\eta = 1$, and no noise, $\sigma_d = 0$, equation 5 turns into $SNR_{bit} = 1/2 \log_2(\mu_p)$, or $SNR = \sqrt{\mu_p}$, which is the pure photon shot noise relation. As a real sensor cannot perform better, the SNR diagram for a real sensor, that is plotted with a red line in figure 3, is always below the photon line, plotted in the same figure with a blue line. When considering a real sensor, two limiting cases

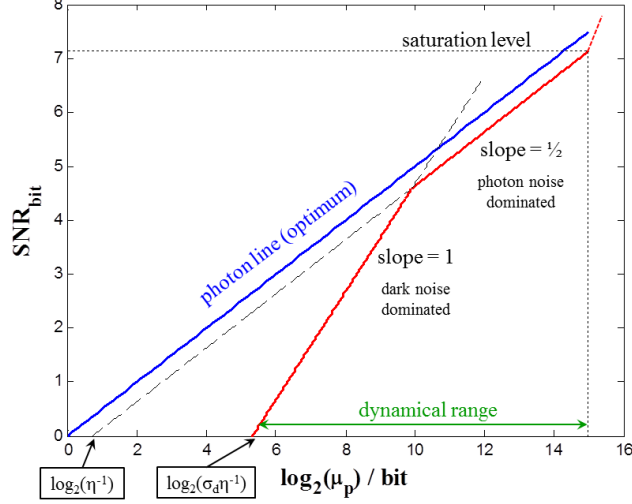


Figure 3: SNR diagram for an ideal (blue) and real (red) sensor

can be taken into account:

- Shot noise dominated: $\eta\mu_p \gg \sigma_d^2$

When the number of incoming photons is high, the dark noise σ_d^2 can be neglected, and the relation seen in eq. 5 can be rewritten as:

$$SNR_{bit} = \frac{1}{2} \log_2(\mu_p) + \frac{1}{2} \log_2(\eta) \quad (6)$$

This part of the SNR plot is a straight line with slope 1/2, which crosses the x-axis in the point $\log_2(\eta^{-1})$ as figure 3 shows, that means the minimum detectable amount of photons (for SNR 1:1) would amount to η^{-1} if the sensor under test had pure shot noise characteristics.

- Dark noise dominated: $\eta\mu_p \ll \sigma_d^2$

For a low number of incoming photons, the dark noise can no longer be neglected, as it would also affect the sensor. Therefore, for very low signal, relation 5 becomes:

$$SNR_{bit} = \log_2(\mu_p) + \log_2(\eta\sigma_d^{-1}) \quad (7)$$

This region of the plot corresponds to a straight line with slope 1, that cuts the x-axis when $\log_2(\mu_p) = \log_2(\sigma_d \eta^{-1})$ (see figure 3). Hence, the minimum detectable signal (SNR 1:1) for a real sensor amounts to $\sigma_d \eta^{-1}$

- Saturation

The last region on the plot corresponds to saturation. If the photon intensity is increased below the photon noise dominated region, saturation is reached, at a corresponding saturation irradiation $\mu_{p,sat}$, with a corresponding saturation capacity of $\mu_{e,sat} = \eta \mu_{p,sat}$.

Saturation means that, for a k-bit digital camera, the digital values from the pixels will be clipped to the maximum digital grey value, $2^k - 1$. The signal clipping causes the variance σ_y^2 to decrease, and SNR_{bit} steeply increases.

From the saturation irradiation and minimum detectable signal, the dynamical range of the sensor (i.e. the ratio between the maximum and minimum signal that is acquired by the sensor) can also be deduced, as shown in figure 3. At the upper limit, pixels appear to be white for every higher value of intensity (saturation), while pixels appear black at the lower limit and below.

Therefore, both Photon Transfer and SNR analysis give access to some important sensor parameters, and will be used in this project to characterize the camera. In the next section, the experimental setup for this characterization will be described.

IV. EXPERIMENTAL PROCEDURE

i. Equipment

The devices used to perform the measurements are:

- Uniform LED light source

The LED light source must be monochromatic (i.e: consisting of a single wavelength) in order to accurately calculate the number of impinging photons, and provide a flat field illumination. In this work a backlight illumination LED RGB Backlight is used, connected to an independent color and intensity ten turn control device [4], seen in figure 5a, which makes it possible to test the camera under different wavelengths.

Only three different colors will be used in the measurement taking, red, green and blue. Each of these spectra was characterised with a spectrometer, being the peak wavelengths: $\lambda_r = 632.86$ nm for red, $\lambda_g = 525.864$ nm for green, and $\lambda_b = 469.408$ nm for blue. The spectra for these wavelengths can be seen in figure 4.

- Power Meter Interface and photodiode

The S130VC Slim diode Power Sensor [5], a silicon photodiode with a ruggedized aluminium head is used to measure the light source power, and connected to the PM101

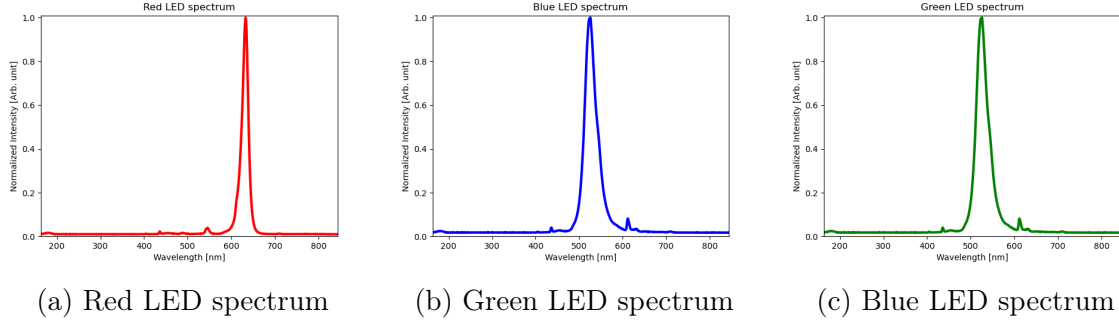


Figure 4: Normalized emitted intensity as a function of the wavelength for the three LED lights measured by the spectrometer



(a) LED light source and control (b) Photodiode used to measure light irradiance and PM 101 device.

Figure 5: Equipment needed in the camera characterisation measurements

interface [6], as figure 5b shows. The interface is connected to the computer via USB, and the power is read by the Optical Power Monitor (OPM) software in the computer.

- Camera

The camera used is the acA2440-20gm Basler ace GigE camera with a Sony IMX264 mono CMOS sensor [7]. Its EMVA parameters, measured at a wavelength of $\lambda = 545\text{nm}$, which will be aimed to reproduce experimentally are:

- Total Quantum Efficiency (QE) : $\eta = 68 \%$
- Inverse of Overall System Gain : $K^{-1} = 2.7 \frac{e^-}{DN}$
- Temporal Dark Noise : $\sigma_{d_0} = 2.3 e^-$
- Saturation Capacity: $\mu_{e,sat} = 10400 e^-$

ii. Setup

The experimental setup can be seen in figure 6.

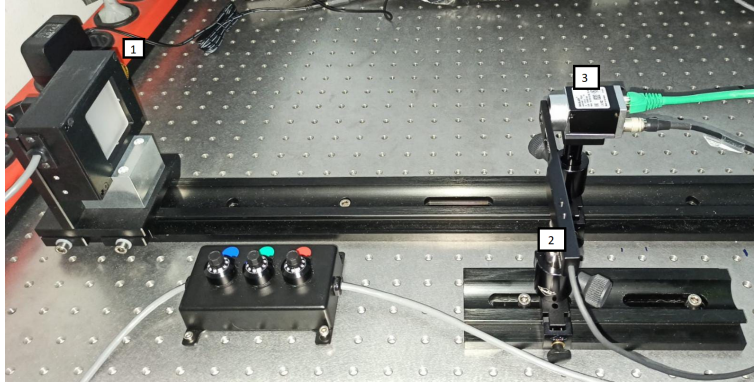


Figure 6: Experimental setup

It consists of a sealed hole table where the LED light source (1), the Thorlabs PM 101 powermeter (2), and the camera (3) are mounted onto two optical benches. This whole setup must be light shielded to ensure only the LED illumination gets to the camera sensor. If a lower irradiance from the light source is desired, neutral density filters can also be placed in front of the LED screen in order to reduce the power that gets to the camera sensor.

The distance between the camera and light source is fixed so that for the lowest chosen exposure time to be used only dark noise is detected (i.e: the whole picture recorded by the camera appears as black), and for the maximal exposure time, the image taken is saturated (i.e: the picture is white). Furthermore, for the chosen distance, the light source must remain homogeneous for all exposure times.

Once the camera is fixed at a certain distance, the power of the LED illumination must be measured using the powermeter. This power can be converted into irradiance I by dividing by the photodiode sensor area, calculated using its diameter ($\varnothing = 9.5$ mm).

$$I = \frac{P}{\pi(\varnothing/2)^2} \quad (8)$$

With knowledge of the exposure time t_{exp} , and the camera *Pixel Size* (not to be confused with the sensor area of the photodiode, which is only used in the power to irradiance conversion), this irradiance can then be transformed into number of incoming photons to the camera, $N_{photons}$.

$$N_{photons} = \frac{I \cdot \lambda \cdot PixelSize \cdot t_{exp}}{hc} \quad (9)$$

This number can be varied by changing the exposure time and keeping the same irradiance. The number of incoming photons must be so that the the range of $\log_2(N_{photon})$ is enough

to cover the whole dynamical range, that is, both the slope 1 region where dark noise dominates (for low $\log_2(N_{photon})$), and the slope 1/2 region where photon noise dominates for $\log_2(N_{photon})$ close to the camera bit depth.

iii. Measurements

The measurement taking is performed using a single Python script that takes care of acquiring the pictures needed for the analysis. During the process, μ_p should be varied. This is done by operating the light at a fixed radiance, and varying the camera t_{exp} , which makes it possible to keep the light at thermal balance. However, this procedure makes it necessary to take a background image for each exposure time in order to determine $\mu_{y,dark}$, as the number of thermally induced electrons contributing to the dark signal linearly depends on t_{exp} .

For each t_{exp} , 20 images are recorded in order to have enough statistical significance to measure the Temporal Noise variance (i.e. the variance between the different values a pixel might get for the same t_{exp}), and a region of interest of 20×20 pixels is selected to be used in the determination of the mean μ_y and total variance σ_y^2

V. ANALYSIS

The measurements presented were performed for two acA2440-20gm Basler ace GigE cameras, and each of them was tested under illumination of three different wavelengths. In this section, only data for one of the wavelengths is shown, as the remaining plots are analogous.

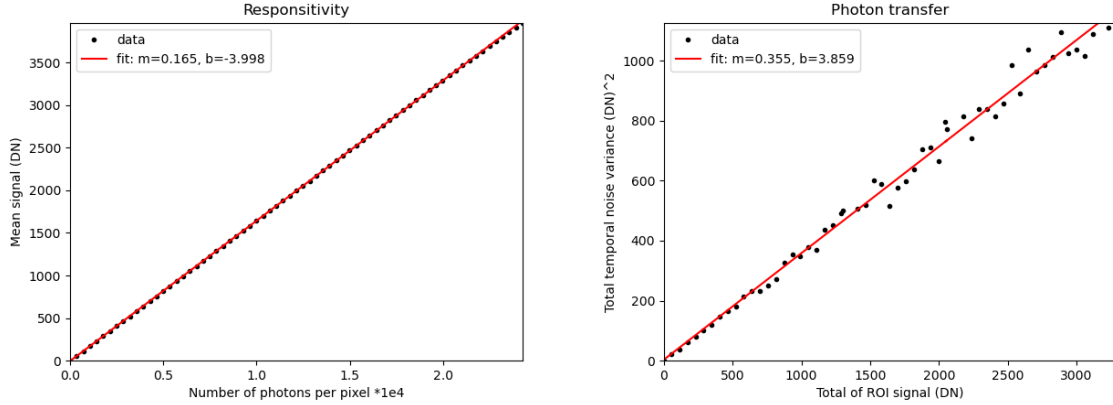
i. Camera 1

Figure 7a shows the responsivity curve for the first camera, when irradiated with red light with wavelength $\lambda_r = 633$ nm. The mean signal is plotted against the photons received per pixel, and it can be seen that the dependence is linear with a strong correlation, which is a desired property for every camera, and also necessary in order to apply the EMVA Standard. Fitting the curve in the region enclosed by minimum intensity and 70 % of saturation capacity to a straight line, the resulting slope is 0.1650 ± 0.0001 . According to equation 1, this value corresponds to $K\eta$.

The same fit is performed for the Photon Transfer curve, which can be seen in figure 7b. The total temporal noise variance σ_y^2 is found to be proportional to the mean signal $\mu_y - \mu_{y,dark}$, however, a large dispersion in the experimental points is found. This is caused by statistical fluctuations in the number of incoming photons. When matched to equation 3 the resulting slope is 0.355 ± 0.006 , which corresponds to K , and the offset is $\sigma_{y,dark}^2 = 3.8 DN^2$. The large fit error in the offset is a consequence of the statistical

fluctuations mentioned earlier, and makes it impossible to get an accurate value for the temporal dark noise from PT measurements.

Together with the response curve, the basic mean parameters temporal dark noise σ_d , inverse system gain K^{-1} and quantum efficiency η can be determined, and compared to the data sheet. This comparison can be seen in Table 1.



(a) Responsivity curve according to Eq.1

(b) PT curve according to Eq. 3

Figure 7: Photon transfer curves for the first camera tested under $\lambda_r = 633$ nm

Furthermore, the above mentioned parameters can also be obtained from a SNR analysis of the same data. The Signal to Noise Ratio plot is shown in figure 8. This figure clearly shows two regions, the first can be described by a straight line with slope 1, and corresponds to a lower signal (which also means lower photon intensity), where, as described in previous sections, dark noise dominates over photon noise. From figure 8, this region is contained approximately in the range between 2 and 5 bits, and is well described by a slope 1 interpolation. The second region can be described with a slope of $\frac{1}{2}$, and corresponds to photon noise dominating over dark noise. A change in the slope can be observed in the region separating the two interpolations. For the range between 9 and 15 pixels, the interpolation function fits the data set well, and the slope resulting from the fit is 0.495, very close to the expected value. Lastly, the saturation region can also be observed, where a steep increase in the SNR happens, caused by the decrease in σ_y^2 when all the pixels reach the maximum digital grey value.

From the intersects with the x axis corresponding to the two different regions mentioned earlier, the quantum efficiency and temporal dark noise can be deduced, using equations 6 and 7. An advantage to using this method is the lower fit error, which makes it accessible to obtain a more accurate value for σ_d . The resulting parameters are shown in table 1.

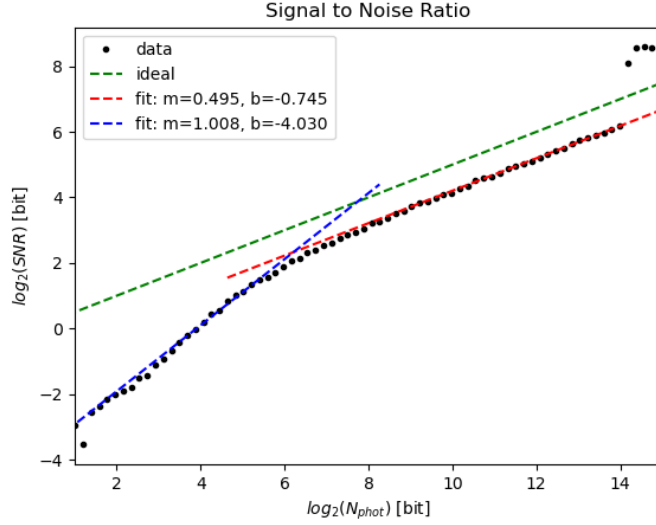


Figure 8: SNR diagram for Camera 1 under a red light where the photon line is marked in a green dashed line, and the slope 1/2 and 1 interpolation are marked in red and blue dashed lines respectively

Wavelength	λ_r		λ_g		λ_b		Data sheet
Item	PT	SNR	PT	SNR	PT	SNR	
η	46 %	36 %	49 %	56 %	50 %	41 %	68 %
K^{-1}	$2.82 \frac{e^-}{DN}$	-	$2.89 \frac{e^-}{DN}$	-	$2.85 \frac{e^-}{DN}$	-	$2.7 \frac{e^-}{DN}$
σ_d	$5.53 e^-$	$5.63 e^-$	$5.21 e^-$	$2.93 e^-$	$5.44 e^-$	$6.30 e^-$	$2.3 e^-$

Table 1: EMVA parameters for camera 1 from PT and SNR analysis for test under three different wavelengths, compared to data sheet. The error in η and K^{-1} is estimated to be in the order of 5 %, and in σ_d in the order of 80 % for PT, and 5% for SNR.

In table 1 the parameters for each wavelength are summarized, and compared to the data sheet. Instead of the overall system gain its reciprocal parameter, K^{-1} is quoted, and noise is expressed in units of e^- instead of DN, which can be converted by multiplication with the inverse system gain.

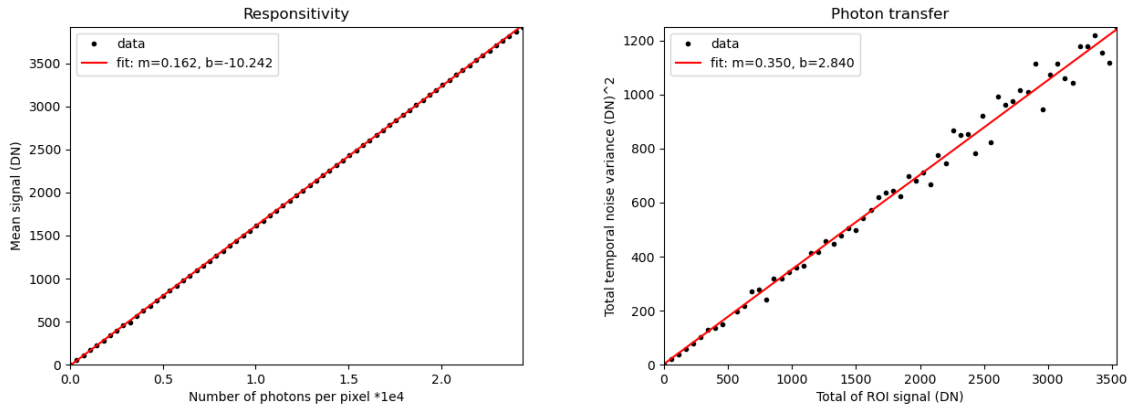
As can be seen in the first row, where the quantum efficiency is quoted, this parameter is found to be lower than its data sheet value for all wavelengths. The reason for this discrepancy could neither be found in the experimental setup, nor in the measurement taking. In addition, the quantum efficiency is wavelength dependent [3], and for the tested camera, η reaches a maximum at a wavelength $\lambda = 545\text{nm}$ [7], which is closest to λ_g . This result is correctly reproduced experimentally, as the highest calculated quantum efficiency corresponds to λ_g .

The temporal dark noise σ_d is also in discrepancy with its data sheet value, as it is experimentally found to be higher under the three considered illuminations, for both the PT and SNR analysis, being the reason for this discrepancy also unknown.

On the other hand, the measured inverse system gain K^{-1} obtained from the PT measurement, is in satisfactory agreement with its data sheet parameter for the three wavelengths.

ii. Camera 2

In order to check the previous results, analysis on a second camera was performed. The data plotted here correspond to irradiation with blue light with wavelength $\lambda_b = 469$ nm. Responsivity and Photon Transfer plots can be seen in figure 9.



(a) Responsivity curve according to Eq.1

(b) PT curve according to Eq. 3

Figure 9: Photon transfer curves for the second camera tested under $\lambda_b = 469$ nm

Both plots are similar to the ones obtained previously for the other camera under the red wavelength. The derived parameters for this camera can be found in table 2. The slope in the responsivity plot is found to be higher, which indicates a higher quantum efficiency, and the points are well aligned in a straight line, which is confirmation for the camera's desired linear response. In the PT plot the data are also well-fitted with a straight line. As the temporal noise variance is caused by dark (i.e. thermally induced) electrons, the linear dependence of the variance with the signal found in figure 9, together with the linear dependence of the signal with t_{exp} found in figure 9a, indicates the number of dark electrons also linearly depends on t_{exp} . The SRN plot is also similar to figure 8, where the dark noise and photon noise dominated regions are clearly distinguishable, and the saturation is reached at about 14.5 bit.

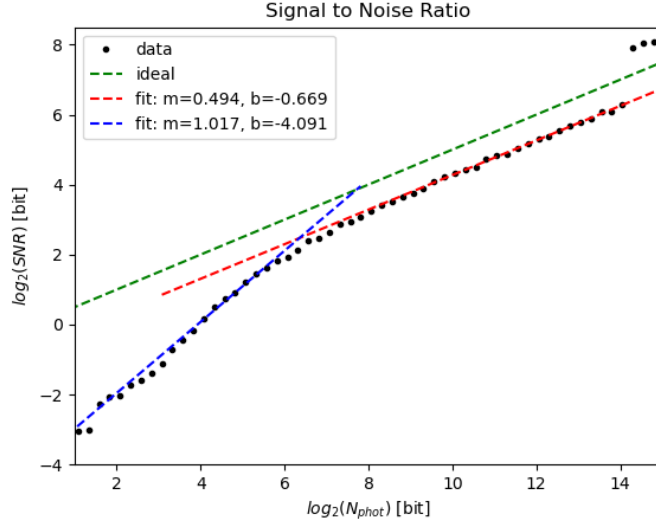


Figure 10: SNR diagram for Camera 2 under a blue light where the photon line is marked in a green dashed line, and the slope $1/2$ and 1 interpolation are marked in red and blue dashed lines respectively

Wavelength	λ_r		λ_g		λ_b		Data sheet
Item	PT	SNR	PT	SNR	PT	SNR	
η	42 %	41 %	46 %	42 %	46 %	40 %	68 %
K^{-1}	$2.82 \frac{e^-}{DN}$	-	$2.9 \frac{e^-}{DN}$	-	$2.86 \frac{e^-}{DN}$	-	$2.7 \frac{e^-}{DN}$
σ_d	$4.54 e^-$	$5.28 e^-$	$8.73 e^-$	$5.88 e^-$	$4.81 e^-$	$2.93 e^-$	$2.3 e^-$

Table 2: EMVA parameters for camera 1 from PT and SNR analysis for test under three different wavelengths, compared to data sheet. The error in η and K^{-1} is estimated to be in the order of 5 %, and in σ_d in the order of 80 % for PT, and 5% for SNR.

VI. CONCLUSIONS

In this report, various camera sensor parameters are derived independently of manufacturer data sheets, based on the analysis of PT and SNR diagrams. The use of this method provides a standard set of parameters that can be used to measure and compare the camera performance. This is an important part in beam diagnostics when working with an accelerator, as it provides a way to make sure the machine's requirements for accuracy are fulfilled, and makes it possible to check whether the data sheet is correct.

For the camera studied in this project, the sensor's linear response is accurately reproduced by the experimental data, and it is also checked that the number of thermally induced electrons contributing to the dark signal linearly depends on the exposure time.

The experimental results found for the camera's quantum efficiency and temporal dark noise do not match the data sheet parameters, although they are of the same order of magnitude. This mismatch is reproduced for two different cameras of the same type, each under three different illuminations; therefore there is a suspicion that a systematic error in the measurement taking could have happened. Nonetheless, the inverse system gain is in satisfactory agreement with its data sheet parameter for both cameras under all illuminations used, which is confirmation for the validity of this method.

In conclusion, the presented method is an accurate, easy to carry out procedure to test a camera's performance and characterize it under a widely used standard. The parameters obtained play an important role in the camera system, and can bring up possible disagreements with that data sheet that should be further checked.

REFERENCES

- [1] G. Kube, Beam diagnostic requirements: an overview (2020). doi:10.48550/ARXIV.2005.08389.
URL <https://arxiv.org/abs/2005.08389>
- [2] B. Walasek-Hoehne, K. Hoehne, R. Singh, Video cameras used in beam instrumentation – an overview (2020). doi:10.48550/ARXIV.2005.04977.
URL <https://arxiv.org/abs/2005.04977>
- [3] Emva standard 1288.
URL <https://www.emva.org/standards-technology/emva-1288/emva-standard-1288-downloads-2/>
- [4] 50 x 50mm metaphase technologies led rgb backlight: Edmund optics.
URL <https://www.edmundoptics.com/p/50-x-50mm-metaphase-technologies-led-rgb-backlight/32399/>
- [5] S130vc slim photodiode power sensor, uv-extended si, 200 - 1100 nm, 50 mw.
URL <https://www.thorlabschina.cn/thorProduct.cfm?partNumber=S130VC>
- [6] Pm101 powermeter manual.
URL <https://seltokphotonics.com/upload/iblock/335/335304ced8d98dfcc57ee450bb04af4a.pdf>
- [7] B. AG, Aca2440-20gm.
URL <https://docs.baslerweb.com/aca2440-20gm>